Protein adsorption in static microsystems: effect of the surface to volume ratio†

Andrea Lionello, Jacques Josserand, Henrik Jensen and Hubert H. Girault*

Received 21st July 2004, Accepted 11th November 2004
First published as an Advance Article on the web 21st December 2004
DOI: 10.1039/b411179f

A numerical model for the adsorption kinetics of proteins on the walls of a microchannel has been developed using the finite element method (FEM) to address the coupling with diffusion phenomena in the restricted microchannel volume. Time evolutions of the concentration of one species are given, both in solution and on the microchannel walls. The model illustrates the adsorption limitation sometimes observed when the microdimensions of these systems induce a global depletion of the bulk solution. A new non-dimensional parameter is introduced to predict the final value of the coverage of any microsystem under static adsorption. A working curve and a criteria ($h/K\Gamma_{max} > 10$) are provided in order to choose, for given adsorption characteristics, the value of the volume-to-surface ratio (*i.e.* the channel height h) avoiding depletion effects on the coverage (relative coverage greater than 90% of the theoretical one). Simulations were compared with confocal microscopy measurements of IgG antibody adsorption on the walls of a PET microchannel. The fit of the model to the experimental data show that the adsorption is under apparent kinetic control.

1 Introduction

Immunoassays, tests that identify a substance (for instance a protein) by its capacity to act as an antigen, are often indicated as a standard tool for the diagnosis of different physiological conditions, from pregnancy to diseases like AIDS or hepatitis. Sometimes these tests are supplied in easy-to-use formats and they can provide a response in a few minutes at best. In fact, in the microtiter well of a standard ELISA, one of the most used immunoassay format, the distances that molecules need to diffuse in order to interact (to adsorb, in the case of the primary antibody) with the solid support are in the order of millimeters. As already illustrated,[1] a large protein like an immunoglobulin G (IgG antibody, 150 kDa) diffuses 1 mm in more than 3 h; diffusion time thus often limits the speed of the analysis. To improve the throughput of immunoassays, the implementation of microfluidics in immunoassays has been proposed.[2] Compared to the classical ones, a micro-immunoassay presents the following advantages: limited reagent consumption and faster analysis time due to a larger surface-to-volume ratio and the improved mass transport efficiency.

Adsorption of macromolecules has proved to be a challenging subject both theoretically and experimentally. Adsorption and transport processes under the Langmuir isotherm assumptions have been modelled mathematically[3] to better understand the phenomena involved in capillary electrochromatography.[4,5] Several models exist for protein mass transfer,[6] for their adsorption on ion exchange particles[7–10] and on sorbent matrices.[11,12] Mathematical models have also been used to describe the adsorption kinetics of proteins[13] and polyelectrolytes[14] on planar surfaces. Computer methods have been employed for decades to study adsorption processes in electrochemical systems characterised by semi-infinite linear diffusion[15,16] in order to get a better understanding of the phenomena involved. A simulation of protein adsorption in a cylindrical geometry from a non-flowing, dilute solution has also been reported.[17] The studies dealing with transport and adsorption of proteins on a substrate define different regimes, depending on the adsorbate–sorbent couple. A diffusional limitation of the processes is observed when the adsorption kinetics is much faster than the diffusion:[18] each protein molecule that reaches the surface is immediately adsorbed and the concentration of analyte near the wall tends to zero. On the other hand, when adsorption is much slower than diffusion controlled mass transport, kinetics plays an important role.[19–21]

In this work, a numerical model using the finite element method has been developed to study adsorption in polymer microchannels in order to describe an allergy test based on an immunoassay. It takes into account the diffusion of one species in the channel, coupled with the adsorption kinetics at the sorbent wall, following the Langmuir isotherm assumptions. It allows the investigation of the mutual influence of the reaction rates, the bulk and the surface concentrations and the solute diffusion coefficient. It provides the time evolution of the concentration in solution and at the surface, revealing how the former can affect the latter in a microsystem. A new non-dimensional parameter characteristic of any microchannel was defined, by which it is possible to calculate the final value of the coverage in that microsystem.

† Electronic supplementary information (ESI) available: Theory: Diffusion–adsorption in the present model, numerical technique, calibration in semi infinite diffusion system (short times). Experimental section: Microchannel fabrication, instrumentation. Results and discussion: Depletion effect. See http://www.rsc.org/suppdata/lc/b4/b411179f/

*hubert.girault@epfl.ch

The study of adsorption of macromolecules has been reported using a variety of measurement techniques, with different protocols and calibrations.[18,22–25] Adsorption kinetics of immunoglobulins in a photoablated polymer microchannel, similar to the ones used in this work, was studied using radiometric detection[18] and by electrochemical detection.[24] The experimental results presented here are obtained by laser-induced-fluorescence confocal microscopy. A confocal microscope was set up[26] and optimised following Ocvirk *et al.*[27] to investigate the adsorption of a fluorescently labelled IgG on PET microchannels. This technique has already been used to study concentration profiles of a "diffusant" in polymer films,[28] adsorption of proteins to chromatographic matrices[29] and to porous adsorbents.[30,31] The detection is made by optical sectioning of the sample. The sample preparation is therefore easier and quicker than for methods requiring mechanical sectioning. It is also a very sensitive method, the high signal-to-background ratio of the set up allowing the detection of very low concentrations.

The finite element simulations are fitted to the experimental results, in order to determine the rates of adsorption. It is questionable[17] whether the adsorption of molecules as heterogeneous as proteins can be described adequately with a few parameters and a general model form. However, if a model can be in accordance with the experimental data in some given conditions, the fitted parameters help to understand the influence of these conditions in order to further optimise them.

2 Theory

Adsorption

The present model is intended for a general case in which a molecule A is adsorbed on a sorbent surface where the active sites B are present. It is based on the Langmuir isotherm model, which uses the active sites concept in the adsorption expression in order to address the reduction of its rate with the coverage of the wall. The model has found wide applications for the adsorption of proteins on substrates or ligands immobilised on a support material.[7,8,11] The Langmuir isotherm model represents a simplified case of protein adsorption, since it assumes (a) reversible adsorption, (b) constant properties of the molecules (proteins) even after the adsorption, (c) no lateral interactions between adsorbed molecules, (d) each active sites B adsorbing only one molecule A and (e) all the adsorption sites having the same affinity for the adsorbate molecules. Although these assumptions are not strictly valid in theory for macromolecular adsorption, the Langmuir model has proven to be useful in practice.[32]

Under such assumptions we can represent the adsorption equation by:

$$\mathrm{A} + \mathrm{B} \underset{k_{on}}{\overset{k_{off}}{\rightleftarrows}} \mathrm{AB} \tag{1}$$

where A is the solute molecule in solution (of bulk concentration C), B is the site active for adsorption on the surface, AB is the adsorbate immobilised (of concentration Γ) onto the active site. The initial surface concentration of the active sites is Γ_{max} (*i.e.* the maximum attainable surface concentration of immobilised adsorbate) and the surface concentration at time t is $\Gamma_{max} - \Gamma(t)$. The constants k_{on} and k_{off} represent the rates of adsorption and desorption of the adsorbate onto the active sites. As a consequence, the kinetics of the process is described by:

$$\frac{\mathrm{d}\Gamma(t)}{\mathrm{d}t} = k_{on} C(t)(\Gamma_{max} - \Gamma(t)) - k_{off}\Gamma(t) \tag{2}$$

The ratio of the constants k_{on}/k_{off} determines the equilibrium constant K (eqn. (3)). Since a monolayer is supposed to be formed, the quantity $\Gamma_{max} - \Gamma(t)$ decreases while $\Gamma(t)$ increases until the equilibrium is reached. At equilibrium $\mathrm{d}\Gamma(t)/\mathrm{d}t = 0$ in eqn. (2) and $C_{eq} = C^{\circ}$ (*i.e.* the initial concentration of A, in cases where the bulk depletion is negligible), leading to eqn. (3). This assumption is consistent with semi-infinite linear diffusion,[15,16] and its validity in the case of a microsystem will be discussed later.

$$K = \frac{k_{on}}{k_{off}} = \frac{\Gamma_{eq}}{C^{\circ}(\Gamma_{max} - \Gamma_{eq})} \tag{3}$$

Eqn. (3) can be written as follows:[16]

$$\frac{\Gamma_{eq}}{\Gamma_{max}} = \frac{KC^{\circ}}{1 + KC^{\circ}} = \frac{\psi}{1 + \psi} \tag{4}$$

where $\psi = KC^{\circ}$. The parameter ψ can be seen as an indicator of the capacity of the system to reach the maximum coverage of the wall. Note that when $\psi \ll 1$ (small coverage of the adsorbent, *i.e.* $\Gamma_{eq} \ll \Gamma_{max}$) this parameter can be neglected in the denominator of eqn. (3) and the adsorption isotherm can be linearised, leading to: $\Gamma_{eq} = KC^{\circ}\Gamma_{max}$.

Diffusion–adsorption (present model)

When the channel is submitted to transient diffusion conditions, the typical flux conservation of the bulk concentration C is given by eqn. (5). The boundary condition at the active wall is expressed by eqn. (6), linking the analyte consumption flux at the active wall to the time evolution of its adsorbed form:

$$\frac{\partial C}{\partial t} + \nabla\bullet(-D\nabla C) = 0 \tag{5}$$

$$\frac{\partial \Gamma}{\partial t} = D\left(\frac{\partial C}{\partial y}\right)_{y=0} = k_{on} C(\Gamma_{max} - \Gamma) - k_{off}\Gamma \tag{6}$$

where D is the analyte diffusion coefficient.

Numerical model

The electronic supplementray information (ESI)† describes how eqn. (5) and (6) are formulated using the FEM method. The following conditions are assumed: (i) The solutions are sufficiently diluted to assume that the variations of the concentration do not modify the viscosity and the density of the fluid, which is also assumed to be uniform. (ii) The channel walls are assumed to be smooth.

Numerical technique

The finite element software Flux-Expert™ (Astek Rhône-Alpes, Grenoble, France) is performed on a Silicon Graphics Octane 2 Unix workstation. The model is formulated in a 2-D Cartesian form and calculations are performed in 1-D and 2-D

geometries as shown in Fig. 1(a) and (b). The model presents 2 regions: the channel containing the bulk solution and the adsorption wall. In the channel, the analyte is characterised by its diffusion coefficient D. Γ_{max}, k_{on} and k_{off} are assigned to the active wall. For all the simulations, a non-linear algorithm based on the Gaussian inversion method has been used. The iterative scheme is performed with a precision criterion of 1% for convergence of the calculation at each time step. The typical time step value is 10^{-2} s even if it was lowered to 10^{-4} s, for high solute concentration. The mesh sizes have been verified to be sufficiently thin not to influence the results. The typical mesh size ranges from 0.1 μm (active layer) to 5 μm (top of the channel) for the validation (Fig. 1a) and from 5 to 20 μm for the comparison with experimental results (Fig. 1b). The initial conditions for transient calculations are: $C = C^\circ$ in the channel and $\Gamma = 0$ in the wall. The physical boundary condition, eqn. (6), being introduced as a consumption term, the only numerical boundary conditions of the model are the Neumann homogeneous ones (no flux) at the non-active walls. For the 1-D calibration (Fig. 1a) the height is sufficient (200 μm) to insure semi-infinite diffusion conditions at the beginning of the adsorption (first 6 s).

Calibration

To validate the model, the simulations are compared with the analytical results for the adsorption kinetics given by Reinmuth for a semi-infinite diffusion system under the Langmuir conditions,[16] and a good agreement was found. (Calibration was done also with the analytical solution for the linear adsorption isotherm[15] with less than 0.6% error.) The simulations are performed with the geometry of Fig. 1a and the values of Table 1. The calibrations can be found in ESI.†

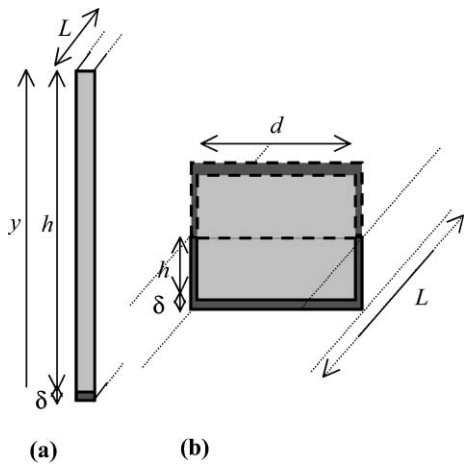

Fig. 1 Schemes of the model, where the diffusion coefficient of the analyte D is defined in the light gray bulk region (of height h), while the initial number of active sites Γ_{max}, the diffusion coefficient to ensure a transversal uniform coverage D', the forward and reverse rates of adsorption k_{on} and k_{off} are assigned to the dark gray wall (of thickness δ). (a) 1-D geometry used for the model validation with $h = 200$ μm and $\delta = 0.1$ μm. (b) 2-D geometry used for comparison with experiments. For symmetry reasons, the adsorbing surface is present on the bottom, the left and the right part of the channel ($h = 50$ μm; $\delta = 5$ μm; $d = 200$ μm).

Table 1 Parameters for the calibration and the experimental comparison. The time of reaction t_{reac} in the calibration case has been calculated for $k_{on} = 2.5 \times 10^8$ m^3 mol^{-1} s^{-1}

Parameters	Calibration	Experimental
D/m^2 s^{-1}	5×10^{-10}	4×10^{-11}
Γ_{max}/mol m^{-2}	3.5×10^{-11}	9.26×10^{-10}
C°/mol m^{-3}	4×10^{-8}–4×10^{-6}	6.67×10^{-6}–10^{-3}
K/m^3 mol^{-1}	2.5×10^6	1.15×10^4
k_{on}/m^3 mol^{-1} s^{-1}	2.5×10^5–2.5×10^9	11.5
k_{off}/s^{-1}	0.1–1000	10^{-3}
t_{max} (elapsed in simul.)/s	6	1800
Γ_{max}'/mol m^{-3} (δ/μm)	3.5×10^{-4} (10^{-7})	1.86×10^{-4} (5×10^{-6})
Parameter ratios	**Calibration**	**Experimental**
$\psi = KC^\circ$	10^{-1}–10	7.7×10^{-2}–11.5
$\vartheta = \frac{4\pi Dt}{K^2\Gamma_{max}^2}$	4.9 at t_{max}	8×10^3 at t_{max}
$t_{diff} = l^2(2D)^{-1}$/s	40	130
$t_{reac} = k_{on}^{-1}C^{\circ\,-1}$/s	1–10^{-3}	1.3×10^4–87
Γ_{eq}/Γ_{max}	6.7×10^{-2}–9×10^{-1}	5.6×10^{-2}–0.89

Table 2 Comparison between the theoretical and the experimental Γ_{eq}/Γ_{max} reached in the microchannel of Fig. 1a. The theoretical Γ_{eq}/Γ_{max} values are calculated from eqn. (4). The experimental Γ_{eq}/Γ_{max} is obtained from simulations run with the geometry of Fig. 1a and the values for the calibration of Table 1 (simulations of Fig. SI1, at longer times)

ψ	Theoretical $\frac{\Gamma_{eq}}{\Gamma_{max}}$	Experimental $\frac{\Gamma_{eq}}{\Gamma_{max}}$	Difference
10	9.09×10^{-1}	9.02×10^{-1}	−0.77%
1	5×10^{-1}	4.51×10^{-1}	−9.8%
0.1	9.09×10^{-2}	6.66×10^{-2}	−26.7%

3 Experimental

The microchannel fabrication has already been described[18,33] and the confocal microscope set up follows ref. 27. Both are fully described in the ESI.†

Reagents and procedure

A 1 mg ml^{-1} (6.67×10^{-6} M) solution of labelled antibody (Fluorolink Cy5 labelled antirabbit IgG, Amersham Pharmacia Biotech) was prepared in deionized water. From this, further solutions were obtained by serial dilutions with 0.01M PBS (SIGMA). The washing buffer is made of a 0.1% Tween-20 (SIGMA) solution in PBS. The adsorption of the fluorolabelled antibody was performed by filling a channel with a drop of 8 μL, placed at the inlet and pushed in with a pipette. After a certain incubation time t, during which adsorption occurs, the channel was emptied by air flushing, and then washed three times with 10 μL of washing buffer. If adsorption times were longer than 3 min, incubation was carried out in a Petri box with a wet tissue inside to avoid evaporation of the drops. As it has been already pointed out,[18] the volume of washing solution is about 100 times that of the channel, which ensures a very efficient washing step. Adsorbed proteins don't desorb or desorb very slowly (hours):[34] consequently we assume that they are not removed during the washing step (the rate of desorption found in this study is

also very slow). The quantity of adsorbed antibody was then measured by the confocal microscope, scanning the channel along the Z-axis: the strongest signal from the channel bottom wall was then collected, representing the adsorbed antibodies. Each channel was used just once. Each mean value and its standard deviation were taken from 5 measurements.

Calibration

To convert the counts from the PMT into concentrations, a calibration curve was drawn with concentration solutions ranging from 3×10^{-9} to 6.67×10^{-6} M. Channels were filled at different concentrations and photons were counted (not shown). At low concentrations, counts and concentrations are proportional (the linear fit was obtained with a regression coefficient of 0.998). The limit of detection of the system is 2×10^{-9} M. At this point, the bulk concentration is multiplied by the volume-to-surface ratio (V/S) of the channel, to have a surface concentration. It is worthwhile emphasising that all the unbound proteins are eliminated from the channel, after three washing steps with an important quantity of buffer.[18] All the proteins measured are adsorbed. Experimental results can now be compared with Γ values from simulations.

4 Results and discussion

4.1 Finite height 1-D diffusion adsorption process

In a microchannel the solution depletes because the solute which adsorbs at the walls is not renewed by semi-infinite diffusion. The bulk concentration value at equilibrium is not C° (as in a semi-infinite diffusion system), but C_{eq} and eqn. (4) should be rewritten as:

$$\frac{\Gamma_{eq}^{\mu syst}}{\Gamma_{max}} = \frac{KC_{eq}}{1+KC_{eq}} \quad (7)$$

The final coverage value $\Gamma_{eq}^{\mu syst}$ is then lower than in an ideal microsystem. This phenomenon is detailed in the ESI.†

Since an effective coverage is suitable in many applications (for instance, a microchannel for ELISA should be uniformly and effectively covered with the primary antibody in order to increase the sensibility of the immunoassay), the general conditions to fulfill in order to avoid depletion have been explored. To do that, the values of coverage at equilibrium in microsystems ($\Gamma_{eq}^{\mu syst}$) obtained from simulations were normalised with the equilibrium coverage value obtained under semi-infinite diffusion (Γ_{eq}^{theor}, from eqn. (4)). This normalised adsorption $\Gamma_{eq}^{\mu syst}/\Gamma_{eq}^{theor}$ was correlated with the initial number of solute moles present in that microsystem ($N^\circ = C^\circ V = C^\circ Ah$, where V, A, h are the volume, the active surface area and the height of the microsystem). To enable a consistent comparison with ideal conditions this quantity was also normalised by the number of moles the wall can theoretically adsorb under semi-infinite diffusion ($N_{wall}^{\infty} = \Gamma_{eq}^{theor} A$). Keeping in mind eqn. (4) the ratio $N^\circ/N_{wall}^{\infty}$ can be written as follows:

$$\frac{N^\circ}{N_{wall}^{\infty}} = \frac{C^\circ h}{\Gamma_{eq}^{theor}} = \frac{h}{K\Gamma_{max}}(1+\psi) = \varphi(1+\psi) \quad (8)$$

where φ ($= h/K\Gamma_{max}$) represents the asymptotic limit of eqn. (8) for $\psi \ll 1$ (*i.e.* very low initial concentration or low K values). The parameter φ is independent of the initial solution concentration and is, consequently, an intrinsic characteristic of any microsystem where adsorption takes place. It represents the lowest possible coverage that can occur in a microsystem in relation to the corresponding ideal system.

The ratio $\Gamma_{eq}^{\mu syst}/\Gamma_{eq}^{theor}$ is represented in Fig. 2 as a function of $N^\circ/N_{wall}^{\infty}$, eqn. (8). Each full line curve represents the normalised adsorption (micro/ideal system) in the function of ψ for a different φ value (*i.e.* a different microsystem).

As just said, the lowest possible abscissa value for each curve is φ. In this way, the dotted line connecting all the φ values

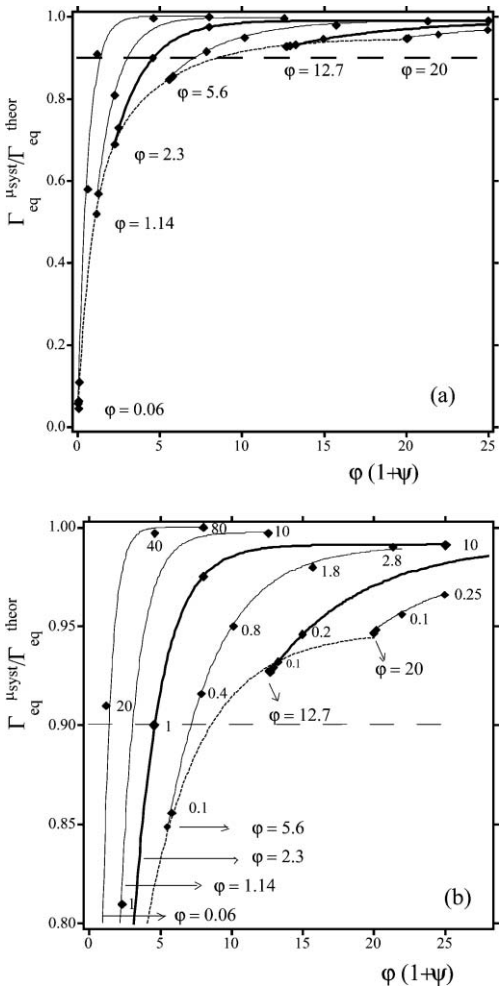

Fig. 2 Working curves to estimate the coverage in a microsystem; the plots show the evolution of the coverage in a microsystem compared to the coverage in the corresponding ideal semi-infinite system in function of ψ and for different values of $\varphi = h/K\Gamma_{max}$. Each full line curve is obtained for increasing values of ψ. The lowest abscissa value of each full line curve corresponds to φ (from left to right φ = 0.06, 1.14, 2.3, 5.6, 12.7, 20) and the corresponding $\Gamma_{eq}^{\mu syst}/\Gamma_{eq}^{theor}$ is the lowest attainable in that microsystem (simulations run with $\psi = 10^{-3}$). The points have been verified for different h (different h values in Fig. 1a), K and Γ_{max} values, changing C° in order to keep ψ constant. The dotted line, connecting all the points with abscissa equal to φ, represents the limit under which the coverage cannot fall in a microsystem characterised by the corresponding φ. Fig. 2(b) is an enlargement of Fig. 2(a) to show the ψ values. The ψ values are written near the corresponding point.

represents the lowest equilibrium coverages that can occur in different microsystems (compared to the theoretical ideal systems).

In Fig. 2b it can be observed that for the same ψ values, $\Gamma_{eq}^{\mu syst}/\Gamma_{eq}^{theor}$ increases with φ. In fact when the volume-to-surface ratio, *i.e.* h is small compared to $K\Gamma_{max}$, the depletion of the solution is very high, and the analyte amount adsorbed at equilibrium is small compared to an ideal system (it can be 0.05% of the corresponding semi-infinite system for $\psi = 0.01$ and $\varphi = 0.06$).

When the h value is high compared to $K\Gamma_{max}$, the microsystem behaviour tends to that of an ideal system: for instance for $\varphi \geqslant 9$ (*i.e.* h is 9 times the product $K\Gamma_{max}$) we can consider of being above the microsystem limitation which is due to the solution depletion, as $\Gamma_{eq}^{\mu syst}/\Gamma_{eq}^{theor}$ is never less than 90% (reachable for $\psi = 0.01$ and less; see horizontal dashed line in Fig. 2).

After having estimated the φ value of a microsystem of interest, the plots in Fig. 2 can be used as working curves to predict the final coverage in that microsystem.

4.2 Isotherm of IgG adsorption on PET

The experimental isotherm of IgG adsorption on photoablated PET microchannels is shown in Fig. 3a, where the Γ_{eq} values are measured at 30 min (corresponding to the final values of the time evolutions of Fig. 3c). The initial solution concentration C° is assumed not to deplete during the adsorption phenomenon, since relatively high C° values are used as shown in Table 1. This assumption is verified with the simulations in the Appendix, since a moderate depletion of the bulk concentration cannot be detected with the confocal microscope. To obtain Γ_{max} and K (necessary for the simulations fitting the experimental kinetics of adsorption shown in Fig. 3c and carried out with the geometry of Fig. 1b), the adsorption isotherm equation (eqn. (3)) is linearised as follows:[35]

$$\frac{C^\circ}{\Gamma_{eq}} = \frac{1}{K\Gamma_{max}} + \frac{C^\circ}{\Gamma_{max}} \quad (9)$$

Γ_{max} and K fitting

The linearised isotherm is reported in Fig. 3b (inside Fig. 3a). Reporting C°/Γ_{eq} *versus* C°, Γ_{max} and K are provided as the respective reciprocals of the slope and the intercept, giving the fitted values $\Gamma_{max} = 9.26 \times 10^{-10}$ mol m^{-2} and $K = 1.15 \times 10^4$ m^3 mol^{-1}. Γ_{max} can also be calculated by taking into account the area of the antibody molecule (14×14 nm[36]), resulting in $\Gamma_{max} = 1.064 \times 10^{-8}$ mol m^{-2}. This estimation implies a compact monolayer of IgG molecules. The deviation from the fitted value can be explained by the fact that PET surface is not so active in physisorption,[37] leading to a decrease of the active sites concentration (in the ratio of 1/10 mol m^{-2}).

Kinetic rates fitting: a reaction-limited case

The IgG adsorption on PET *versus* the incubation or adsorption time t is given in Fig. 3c (markers) for different antibody concentrations. The corresponding simulations, represented by lines, are performed with the geometry of Fig. 1b. The

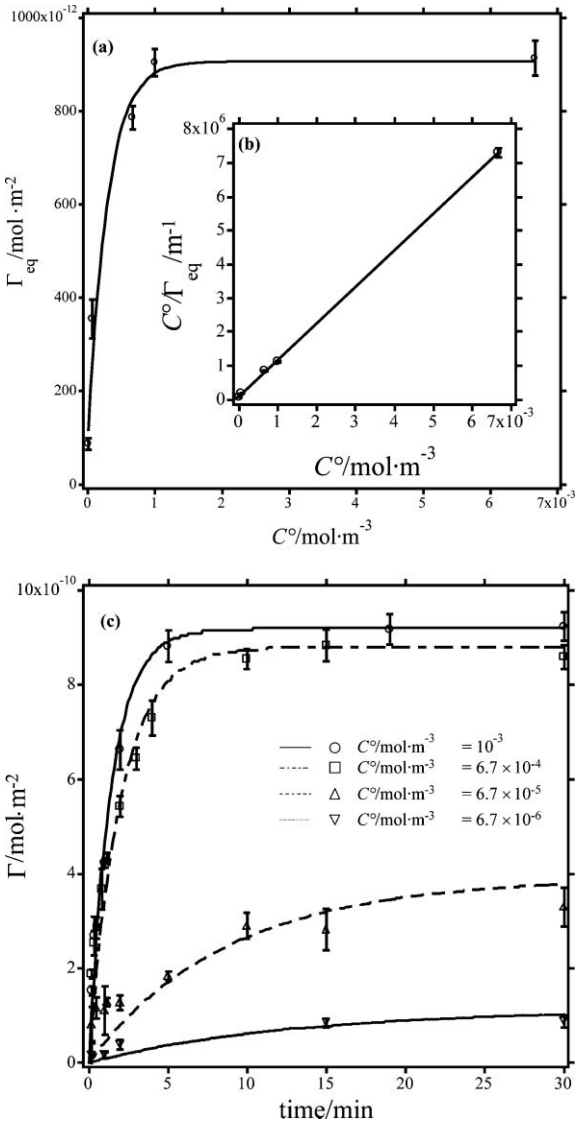

Fig. 3 (a) Isotherm of adsorption of anti-rabbit IgG on laser-ablated PET obtained from the experimental results at 30 min of Fig. 3c. The fit has the sole purpose of illustrating the trend of the isotherm. (b) (inside) Linearization of the adsorption isotherm, following eqn. (9): regression coefficient = 0.999, slope = 1.08×10^9 m^2 mol^{-1}, intercept = 9.40×10^4 m^{-1}, from which $\Gamma_{max} = 9.26 \times 10^{-10}$ mol m^{-2} and $K = 1.15 \times 10^4$ m^3 mol^{-1}. (c) Simulations (lines) compared with experimental results (markers). Calculations are run with $D = 4 \times 10^{-11}$ m^2 s^{-1}, $\Gamma_{max} = 9.26 \times 10^{-10}$ mol m^{-2}, $K = 1.15 \times 10^4$ m^3 mol^{-1} ($k_{on} = 11.5$ m^3 mol^{-1} s^{-1} and $k_{off} = 10^{-3}$ s^{-1}). The initial concentrations for experiments and simulations are $C^\circ = 10^{-3}$, 6.67×10^{-4}, 6.67×10^{-5}, and 6.67×10^{-6} mol m^{-3}.

parameters for simulations are reported in Table 1. The kinetics rates obtained from the experimental fitting are far below the diffusion limitation ones ($k_{off} = 10^{-3}$ s^{-1} instead of the [1–100] s^{-1} range for near diffusion control).

An evaluation of the conditions corresponding to limitations by diffusion or kinetics can be done.[38] In Table 1 we compare the characteristic reaction time $t_{reac} = 1/k_{on}C^\circ$ with the typical time of diffusion $t_{diff} = h^2/2D$, where h is the diffusion length (the values used are those of Fig. 3c). The time t_{diff} equals 130 s

while t_{reac} varies from 87 s (higher C° in Fig. 3c) to about 3.6 h (lower C°): in the first case (high C°), the reaction occurs in the same time order as diffusion, resulting in a mixed regime. At lower concentrations, the reaction is so slow that only a small amount of antibodies is adsorbed, leading to a near-wall C value just below C°. Simulations of the concentration show a weak gradient profile across the channel, which is established in some minutes because the kinetics slows the process down (for comparison, the gradient shown in Fig. SI1† for pure diffusional control is established in 0.1 s).

Protein adsorption controlled by kinetics was reported several times. Van Dulm and Norde[19] explained slow adsorption of albumin on negatively charged polystyrene with the fact that albumin molecules have to cross an energy barrier caused by overlapping electric fields from the negative charges on the sorbent and the protein. Wojciechowski *et al.*[20] found a similar behaviour for adsorption of fibrinogen on various surfaces. In an extensive study of adsorption of different proteins on different substrates, Young, Pitt and Cooper[21] found a kinetic limited process for IgG adsorption on polyvinyl chloride, polyethylene and polyether polyurethaneurea. Again, the existence of an energy barrier is given to explain this kind of limitation, also encountered in our system.

Antibody adsorption on bare substrates is the most simple and one of the most popular immobilization methods, even if it leads to low surface coverage and low activity of the physisorbed antibodies.[37] To overcome this limitations adsorption in gels,[39,40] porous media[31,41] or bead-beds[42] are often used to enhance the coverage.

5 Conclusions

The time evolution of the wall adsorption of one species in 1D and 2D microsystems has been studied under static conditions. The employed finite element model considers the diffusion of the species in solution, coupled to the adsorption kinetics on the sorbent surface. The analyte diffusion coefficient, the density of the active sites present on the surface and the kinetic rates of adsorption and desorption are taken into account. The model has been validated under diffusion control by comparison with analytical models of the Langmuir isotherm.

It is observed that the adsorption can be limited by the depletion of the bulk solution, due to the micro-dimensions of the system. Accordingly, for low initial solution concentrations, the coverage values at equilibrium can be markedly lower than the theoretical ones. A working curve and a new non-dimensional parameter ($\varphi = h/K\Gamma_{max}$) are provided in order to predict the depletion effect on the coverage values in any static situation. To overcome the limitations induced by the microdimensions, the channel height h (*i.e.* the volume-to-surface ratio) must be higher than $10K\Gamma_{max}$, insuring 90% of the coverage obtainable in a semi-infinite diffusion system: small h values can be compensated by high concentrations. Further work will consider different ways of renewing the solution in order to reach the full coverage in a microsystem.

Adsorption of fluorescently labelled IgG antibodies on the walls of a laser ablated PET microchannel was measured by a purpose-built simple and very sensitive confocal microscope.

Table 3 Comparison between the theoretical and the experimental Γ_{eq}/Γ_{max} attainable in the microchannel used for comparison with experiments (Fig. 1b). The experimental Γ_{eq}/Γ_{max} deviates more from the theoretical one as C° is lowered. C_{eq} follows the same behaviour, deviating from C°

C°/mol m^{-3}	Theoretical $\frac{\Gamma_{eq}}{\Gamma_{max}}$	Experimental $\frac{\Gamma_{eq}}{\Gamma_{max}}$	Difference (%)	C_{eq}/C°
10^{-3}	0.92	0.89	3.3	98%
6.67×10^{-4}	0.88	0.86	2.3	97%
6.67×10^{-5}	0.43	0.38	11.6	86%
6.67×10^{-6}	0.071	0.056	21.1	81%

Fitting the simulations to the experimental time evolution reveals a kinetic controlled adsorption.

Appendix

Depletion effect: validity remark

In Table 3 the ratios Γ_{eq}/Γ_{max} obtained from simulations are compared with the theoretical ones, calculated from eqn. (4). The values are similar only for the higher C° values, due to the depletion occurring in this microsystem (h = 50 μm). Indeed, at low C°, the initial assumption ($C_{eq} = C^\circ$) is not valid: therefore, the true values of C_{eq} from simulations at 30 min are employed to determine a new isotherm of adsorption in function of C_{eq} (not shown). For this, eqn. (9) is rewritten by replacing C° with C_{eq}. This isotherm provides 0.2% and 4% deviation for Γ_{max} and K respectively, confirming the validity of previous fitted values used for Fig. 3c.

Acknowledgements

Thanks to Dr Joel S. Rossier (DiagnoSwiss S.A., CH) for the helpful reading of the manuscript. The Research Program UE 1.1–LIFE–GENERIC (Project: "MICROPROTEOMICS: New microfluidic-mass spectrometry technologies for high performance proteomics" N° OFES '01.1821) is gratefully acknowledged for financial support.

Andrea Lionello, Jacques Josserand, Henrik Jensen and Hubert H. Girault*

Laboratoire d'Electrochimie Physique et Analytique, Institut des Sciences et Ingénierie Chimiques (ISIC), Ecole Polytechnique Fédérale de Lausanne, CH-1015 Lausanne, Switzerland.

E-mail: hubert.girault@epfl.ch; Fax: +41 21 693 36 67; Tel: +41 693 31 51

References

1 A. Dodge, K. Fluri, E. Verpoorte and N. F. de Rooij, *Anal. Chem.*, 2001, **73**, 3400–3409.
2 L. B. Koutny, D. Schmalzing, T. A. Taylor and M. Fuchs, *Anal. Chem.*, 1996, **68**, 18–22.
3 K. Mondal and S. B. Lalvani, *Sep. Sci. Technol.*, 2000, **35**, 2583–2599.
4 M. Paces, J. Kosek, M. Marek, U. Tallarek and A. Seidel-Morgenstern, *Electrophoresis*, 2003, **24**, 380–389.
5 S. Golshanshirazi and G. Guiochon, *Anal. Chem.*, 1988, **60**, 2364–2374.
6 R. W. Glaser, *Anal. Biochem.*, 1993, **213**, 152–161.
7 G. L. Skidmore, B. J. Horstmann and H. A. Chase, *J. Chromatogr.*, 1990, **498**, 113–128.
8 Q. D. Lan, A. S. Bassi, J. X. Zhu and A. Margaritis, *Chem. Eng. J.*, 2001, **81**, 179–186.

9 Q. M. Mao, R. Stockmann, I. G. Prince and M. T. W. Hearn, *J. Chromatogr.*, 1993, **646**, 67–80.
10 G. E. Rowe, A. Margaritis, Q. Lan, A. S. Bassi and J. X. Zhu, *Biotechnol. Bioeng.*, 1999, **65**, 613–621.
11 B. J. Horstmann and H. A. Chase, *Chem. Eng. Res. Des.*, 1989, **67**, 243–254.
12 B. J. Horstmann and H. A. Chase, *Bioseparation*, 1998, **7**, 145–157.
13 M. A. McCoy and A. I. Liapis, *J. Chromatogr.*, 1991, **548**, 25–60.
14 L. K. Filippov and N. L. Filippova, *J. Colloid Interface Sci.*, 1997, **189**, 1–16.
15 P. Delahay and I. Trachtenberg, *J. Am. Chem. Soc.*, 1957, **79**, 2355–2362.
16 W. H. Reinmuth, *J. Phys. Chem.*, 1961, **65**, 473–&.
17 P. W. Wojciechowski and J. L. Brash, *J. Colloid Interface Sci.*, 1990, **140**, 239–252.
18 J. S. Rossier, G. Gokulrangan, H. H. Girault, S. Svojanovsky and G. S. Wilson, *Langmuir*, 2000, **16**, 8489–8494.
19 P. Vandulm and W. Norde, *J. Colloid Interface Sci.*, 1983, **91**, 248–255.
20 P. Wojciechowski, P. Tenhove and J. L. Brash, *J. Colloid Interface Sci.*, 1986, **111**, 455–465.
21 B. R. Young, W. G. Pitt and S. L. Cooper, *J. Colloid Interface Sci.*, 1988, **125**, 246–260.
22 U. Reichert, T. Linden, G. Belfort, M. R. Kula and J. Thommes, *J. Membr. Sci.*, 2002, **199**, 161–166.
23 M. C. Davies, R. Green, X. Y. Chen, C. J. Roberts, K. M. Shakesheff, S. S. B. Tendler and P. M. Williams, *Abstr. Pap.-Am. Chem. Soc.*, 1995, **209**, 6-POLY.
24 J. S. Rossier and H. H. Girault, *Lab Chip*, 2001, **1**, 153–157.
25 P. Schaaf and P. Dejardin, *Colloids Surf.*, 1988, **31**, 89–103.
26 F. Bianchi, EPFL, Lausanne-Switzerland, 2001.
27 G. Ocvirk, T. Tang and D. J. Harrison, *Analyst*, 1998, **123**, 1429–1434.
28 E. G. McFarland, S. Michielsen and W. W. Carr, *Appl. Spectrosc.*, 2001, **55**, 481–489.
29 A. Ljunglof and J. Thommes, *J. Chromatogr. A*, 1998, **813**, 387–395.
30 A. Ljunglof and R. Hjorth, *J. Chromatogr. A*, 1996, **743**, 75–83.
31 T. Linden, A. Ljunglof, M. R. Kula and J. Thommes, *Biotechnol. Bioeng.*, 1999, **65**, 622–630.
32 E. C. Moreno, M. Kresak, J. J. Kane and D. I. Hay, *Langmuir*, 1987, **3**, 511–519.
33 M. A. Roberts, J. S. Rossier, P. Bercier and H. Girault, *Anal. Chem.*, 1997, **69**, 2035–2042.
34 C. E. Giacomelli, M. J. Avena and C. P. DePauli, *J. Colloid Interface Sci.*, 1997, **188**, 387–395.
35 D. Mazzone, Università degli studi di Genova, 1998.
36 R. J. Green, J. Davies, M. C. Davies, C. J. Roberts and S. J. B. Tendler, *Biomaterials*, 1997, **18**, 405–413.
37 J. N. Lin, I. N. Chang, J. D. Andrade, J. N. Herron and D. A. Christensen, *J. Chromatogr.*, 1991, **542**, 41–54.
38 T. Mason, A. R. Pineda, C. Wofsy and B. Goldstein, *Math. Biosci.*, 1999, **159**, 123–144.
39 J. C. Vazquez-Lira, E. Camacho-Frias, A. Pena-Alvarez and L. E. Vera-Avila, *Chem. Mater.*, 2003, **15**, 154–161.
40 H. Mansur, R. Orefice, M. Pereira, Z. Lobato, W. Vasconcelos and L. Machado, *Spectrosc.: Int. J.*, 2002, **16**, 351–360.
41 G. M. S. Finette, Q. M. Mao and M. T. W. Hearn, *J. Chromatogr. A*, 1997, **763**, 71–90.
42 K. Sato, M. Tokeshi, T. Odake, H. Kimura, T. Ooi, M. Nakao and T. Kitamori, *Anal. Chem.*, 2000, **72**, 1144–1147.

